http://dx.doi.org/10.1016/j.jsv.2020.115733

Mode-mismatching Enhanced Disbond Detection Using Material Nonlinearity in Guided Waves at Low Frequency

Kai WANG[a], *Menglong LIU*[b] *, *Zhongqing SU*[c], *Shifeng GUO*[d,e], *Fangsen CUI* [f]

[a] Interdisciplinary Division of Aeronautical and Aviation Engineering, The Hong Kong Polytechnic University, Kowloon, Hong Kong SAR

[b] School of Mechanical Engineering and Automation, Harbin Institute of Technology, Shenzhen 518052, P.R. China

[c] Department of Mechanical Engineering, The Hong Kong Polytechnic University, Kowloon, Hong Kong SAR

[d] Guangdong Provincial Key Laboratory of Robotics and Intelligent System, Shenzhen Institutes of Advanced Technology, Chinese Academy of Sciences, Shenzhen 518055, China

[e] Chinese Academy of Science Key Laboratory of Human-Machine-Intelligence Synergic Systems, Shenzhen Institutes of Advanced Technology, Chinese Academy of Science, China

[f] Institute of High Performance Computing, A*STAR (Agency for Science, Technology and Research), 138632, Singapore

submitted to ***Journal of Sound and Vibration***

(Initial submission on 22 September 2019; Revised and re-submitted on 2 August 2020)

* To whom correspondence should be addressed.
Email: liumenglong@hit.edu.cn (Dr. M. LIU)

Nomenclature

Al	aluminum
CAN	contact acoustic nonlinearity
FEA	finite element analysis
NDE	nondestructive evaluation
RANP	relative acoustic nonlinear parameter
SHM	structural health monitoring
SOHW	second-order harmonic wave
STFT	short-time Fourier transform
TOE	third-order elastic modulus
UGW	ultrasonic guided wave

Abstract

Disbond defect is a critical concern for the integrity of adhesively bonded engineering structures, and its characterization using ultrasonic guided waves (UGW)-based methods, suffers from the contradiction of multiple wave modes co-excitation at high frequency and poor sensitivity at low frequency. With this concern, this study addresses an investigation of disbond-disturbed nonlinearity in ultrasonic guided waves (UGWs) at low frequency, and on this basis, a novel disbond detection method is developed featuring enhancement by the mode-mismatching between fundamental and second-order harmonic wave (SOHW) at a specific mode-frequency combination. First, when the probing UGWs at low frequency are excited in adhesive bonded waveguide (aluminum-epoxy-aluminum), the SOHW in intact waveguides and the disbond region are scrutinized from analytical and numerical perspectives. It is observed that in the case of mode-mismatching for UGW of a specific mode-frequency combination, SOHW is remarkably suppressed in intact regions, whereby leading to the predominance of the disbond-induced SOHW. Then, on this basis, a nonlinearity-based method using the UGW with specific mode-frequency combination is developed to outstand the disbond defect. Finally, the experimental evaluation of disbonds well validates the effectiveness of the proposed method, in which three disbond defects with various lengths (10 mm, 20 mm, and 40 mm) are identified and quantitatively evaluated using the optimal UGW mode-frequency combination.

Keywords: ultrasonic guided waves; adhesive bonded waveguide; disbond detection; material nonlinearity; second-order harmonic wave

1. Introduction

Adhesive bonding is a prevalently adopted connecting technique in engineering applications [1–3], enabling the construction of stronger and lighter structures. The inappropriate surface preparation in the manufacturing process, the fatigue loading and adverse environment in service can lead to the bonding degradation and further disbond defect, which might result in structural failures and even catastrophes. Exemplarily, a Boeing 737-200 owned by Aloha Airlines, experienced an explosive decompression and structural failure at 24,000 feet, on April 28, 1988, leading to one fatality and vast economic loss. Later investigation [4] has revealed that the failure of a lap joint and the separation of the fuselage upper lobe, initiated by the presence of significant disbond and fatigue damage, was the culprit of this disaster.

With the recognition of the importance of bonding quality, numerous nondestructive evaluation (NDE) and structural health monitoring (SHM) methods [5–7] have been developed. Among these methods, disbond evaluation using ultrasonic guided waves (UGWs) has attracted intensive research efforts [8], owing to the merits of UGWs in comparison to ultrasonic bulk waves used in conventional methods including: (1) its capacity to inspect a large area, enhancing the evaluation efficiency dramatically; (2) the applicability on thin plates to which bulk wave might be ineffective; and (3) access to hidden structural components. Conventionally, the disbond-induced changes in linear features of probing UGWs have been intensively studied [9–17]. On this basis, UGWs of specific mode-frequency combination, with large out-of-plane shear stress at the adhesive-adherend interface [15] or large out-of-plane displacement at the adhesive layer [16], have been selected to perform disbond detection. For disbond detection, a higher

frequency is preferred as it corresponds to a smaller wavelength, and thus implies a higher sensitivity to disbond. For instance, the authors exhausted themselves selecting UGW mode 11 at 3.85 MHz to quantitatively detect disbond size of an aluminum-epoxy-aluminum bonded joint [17]. However, the preferred UGW suffers from the interference from other co-generated multiple UGW modes, which perplexes the signal processing and result interpretation. On the contrary, UGW mode at a low frequency that features convenience in isolation and interpretation is usually not advocated, as it implies an insensitivity to disbond as the corresponding wavelength is large. This contradiction acts as a key factor impeding the application of UGW to disbond detection.

Compared with linear features, nonlinear features of ultrasonic waves have been proven to be more sensitive to defect of small scale, and have recently been studied for the evaluation of bonding degradation or kissing bond [18, 19]. At the core of recent researches is the evaluation of the kissing bond. It is assumed in [19] that the traversing waves induce a bi-linear stiffness response or the opening and closing of the contact interface at the kissing bond, and this leads to the generation of contact acoustic nonlinearity (CAN) in probing ultrasonic waves [20–25]. On this basis, by calibrating the CAN in probing UGWs, the bonding degradation can be assessed. Nevertheless, the generation of CAN requires a large excitation force to trigger the opening/closing of the disbond surfaces that are initially in a closed status [20], and hence the effectiveness of CAN-based method is prone to the influence of external loading on the waveguide and the working conditions. More importantly, the defect-induced nonlinearity in UGWs is usually weak, making it challenging to extract the defect-induced nonlinearity from that induced by the intact waveguide.

To make use of the UGW at low frequency that features easiness in isolation and to outstand the disbond-induced nonlinearity, a method based on another form of nonlinear UGW, whose generation is attributable to the disbond-induced structural characteristic, is developed, in which the mode-mismatching for specific mode-frequency combination is utilized. In the disbonded region, the structural features are distinct from those in the intact region, i.e. the bonded waveguide retreats to two separated waveguides that guide the wave propagation independently. The properties of wave propagation (e.g. phase/group velocity, wave modality) in each waveguide in the disbonded region are remarkably different from those propagating in the intact bonded region. Consequently, this difference can alter the generation of nonlinear traits in probing UGWs. Nevertheless, the nonlinear traits induced by the disbond-related structural characteristic are rarely reported up to date.

To investigate the disbond-induced changes in nonlinear wave features, a comprehensive theoretical analysis, together with numerical model, interpreting the mechanism behind the generation of second-order harmonic wave (SOHW) in UGWs in disbonded region is established. With this interpretation, an optimal mode-frequency combination of UGW featuring mode-mismatching can be selected, which does not satisfy the requirements of internal resonance [26]. With this optimal mode, the nonlinearity of UGWs induced by intact waveguide can be substantially suppressed, and thereby the disbond-induced SOHW dominates the UGWs. On this basis, an approach which enables outstanding and assessing the disbond-induced nonlinearity is proposed to evaluate the bonding quality and characterize the disbond defect. The merit of the proposed approach lies in the novel exploitation of the differences between material nonlinearity-related wave behaviors in the bonded pristine region and the disbond region. Unlike the CAN, the proposed

approach in this study does not require the interaction between disbond surfaces, and therefore it can usher a novel avenue for the characterization of disbond defect and applies to more general cases of disbond (including kissing disbond), where there exists a narrow gap in the order of micro meter, as evidenced in several reports [27, 28].

The rest of the paper is organized as follows. Section 2 briefly introduces the phase/group velocity and wave structure characteristics in the bonded/disbonded waveguide, which is followed by the numerical modeling (Section 3) of nonlinear features of UGWs in both intact and disbonded waveguides. Section 4 presents the experimental validation of nonlinearity of UGWs in both intact and disbonded waveguides, in which an optimal mode-frequency combination featuring mode-mismatching is exploited for disbond evaluation. Concluding remarks are summarized in Section 5.

2. Dispersion Curve

To investigate the linear/nonlinear features of UGW in the bonded waveguide, the dispersion properties of UGWs are analyzed first, which serves as the cornerstone for analysis of nonlinear feature generation and for interpretation of results in the following numerical investigation and experiments. The wave propagation in Al-epoxy-Al (with thickness 1 mm-0.2 mm-1 mm) bonded waveguide with disbond defect is illustrated schematically in Figure 1, wherein a disbond defect is modeled with unbonded surfaces between the adhesive and the adherend, which transmit no shear stress. In this scenario, the waveguide includes three regions, *i.e.* the intact bonded region denoted R_1 (Al-epoxy-Al), the upper part of disbonded region denoted R_2 (Al), and the lower part of disbonded region denoted R_3 (epoxy-Al). In these three distinct regions, guided waves propagate with different characteristics in terms of phase/group velocity dispersion curves

and wave structure in the thickness direction.

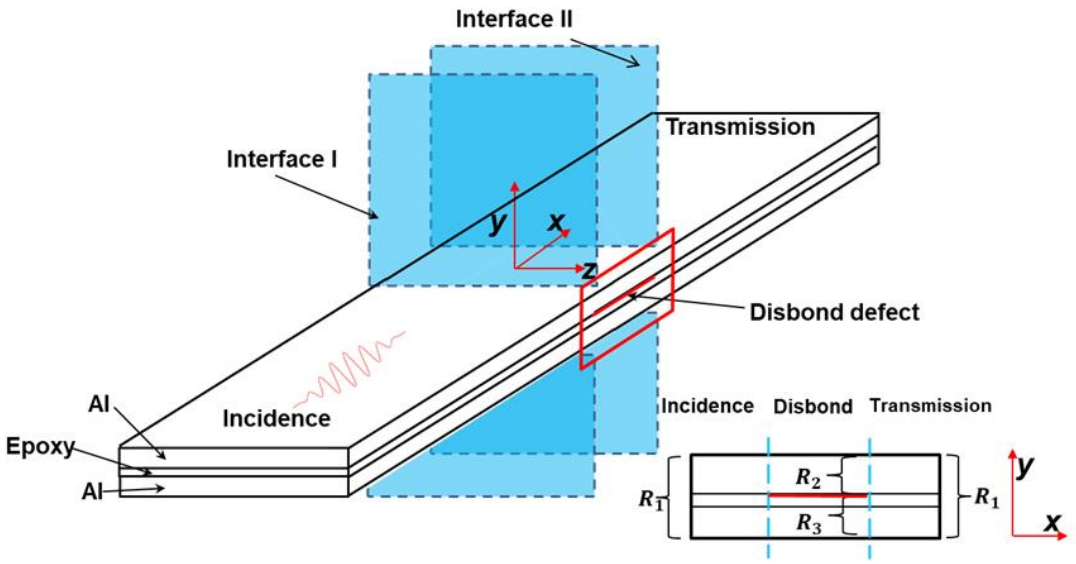

Figure 1 Illustration of wave propagation in Al-epoxy-Al (thickness 1 mm – 0.2 mm – 1 mm) bonded waveguide with disbond defect.

Given the material parameters listed in Table 1, the stress-strain relation in one-dimensional scenario can be expressed as $\sigma = (E + E_2\varepsilon)\varepsilon$,where $E_2 = (3E + 2\mathcal{A} + 6\mathcal{B} + 2\mathcal{C})/2$, to generate the nonlinear stress-strain curve as displayed in Figure 2. It can be seen that the nonlinearity gradually stands out at large strain, and it is this nonlinear stress-strain relation that leads to the generation of nonlinear wave features (e.g. SOHW).

Table 1 Material parameters for Al and epoxy.

Part	Thickness (mm)	Elastic modulus (GPa)	Poisson's ratio	Density (kg/m^3)	$\mathcal{A}$ (GPa)	$\mathcal{B}$ (GPa)	$\mathcal{C}$ (GPa)
Aluminum	1	68.9	0.33	2780	−320	−200	−190
Epoxy	0.2	1.8	0.402	1104	-8.36	-5.22	-4.96

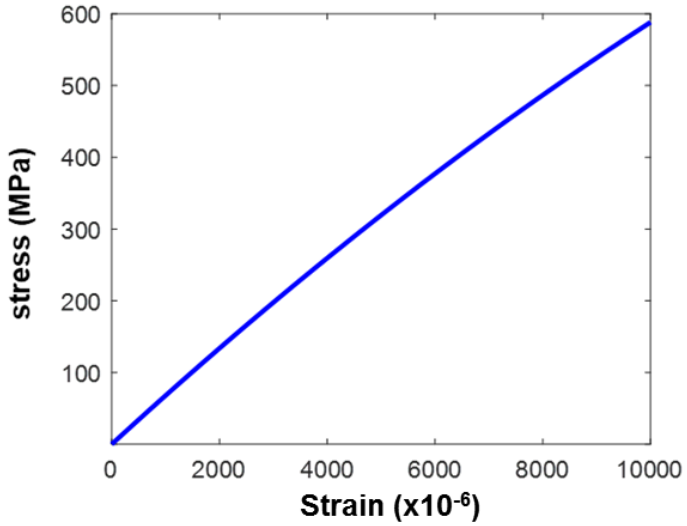

Figure 2 Nonlinear stress-strain curve in one-dimensional scenario with material parameters in **Table 1**.

Phase and group velocity dispersion curves of UGWs in all the three regions, namely Al-epoxy-Al (R_1), Al (R_2), and epoxy-Al (R_3), can be obtained with the global matrix method [29], as shown in Figure 3. The modes in region R_2 (single layer waveguide) are denoted by the S_0 and A_0 to be consistent with other investigations, and the modes in R_1 and R_3 regions (multi-layer waveguide) are denoted by numbers in black and blue, respectively, to differentiate them from those in region R_2. $\mathcal{A}$, $\mathcal{B}$, and $\mathcal{C}$ in Table 1 are the third-order elastic (TOE) modulus which lead to the generation of nonlinear features of UGWs and hence not used for calculation of dispersion curve. From the obtained dispersion curves (see Figure 3), the phase/group velocities between R_2 and R_3 are observed almost coincident, which arises from the fact that the epoxy layer in R_3 is such thin that it exerts an insignificant influence on the overall dispersion characteristic of UGWs in R_3. It is clearly demonstrated that at some specific frequencies, the phase velocity curves of different modes in R_1, R_2, and R_3 almost overlap, while at other frequencies, remarkable discrepancies between the phase velocity curves in R_1 and those in R_2 and R_3 are manifested. These discrepancies lead to the fact that at certain incident frequencies,

the internal resonance requirements are satisfied only in the defect regions, and thus only the nonlinear features generated in the defect regions are accumulative. Therefore, the disbond defect can induce remarkable changes in the nonlinear wave features when UGWs at these incident frequencies are used. This provides the theoretical cornerstone for this investigation.

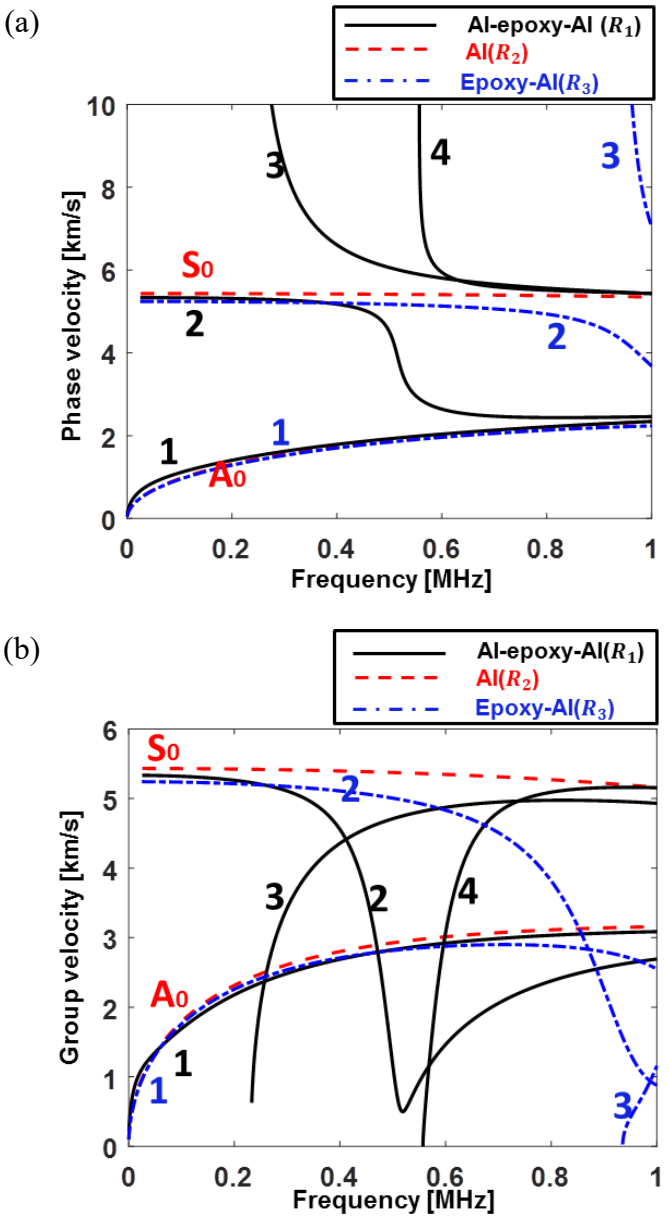

Figure 3 Velocity dispersion curves of UGWs in different regions of bonded Al-epoxy-Al waveguide with disbond defect (a) phase velocity and (b) group velocity.

3. Nonlinearity in UGWs – Numerical Modeling

With the ascertained dispersion curves of each UGW mode, numerical simulation is to be performed to explore the nonlinear features induced by intact waveguide and to interrogate the disbond-induced SOHW in UGWs.

3.1.Simulation Setup

Consider a multi-layer bonded waveguide identical to that shown in Figure 1, which is composed of two aluminum plates (with thickness of 1 mm) bonded by an epoxy film (with thickness of 0.2 mm), a dedicated modeling technique is developed and implemented using the finite element analysis (FEA) via Abaqus®/Explicit. As CAN can be barely excited for disbond with a narrow gap in the order of micrometer, the generation of nonlinear features of UGWs, typified by high order harmonics, is mainly attributed to the intrinsic material nonlinearity.

Considering that higher frequency indicates the excitation of more UGW modes, perplexing the corresponding analysis, the frequency of interest is limited to the range from 0.10 MHz to 0.45 MHz to concentrate the study within first four modes in the bonded waveguide. Mode 2 in this frequency range features a high propagation velocity compared with other modes, enabling an easy separation from other propagating modes, thus it is selected as the incident fundamental wave.

In the built 2-D plane strain model, the incident frequencies are swept from 0.10 MHz to 0.45 MHz, with an increment of 0.025 MHz, to gain an insight into the generation of SOHW in the intact multi-layer region, as well as in the disbond region. The modeling of material nonlinearity is realized by substituting the stress-strain relation in the calculation

process of the Abaqus®/Explicit with a specifically defined nonlinear stress-strain relation via user subroutine VUMAT developed by the authors [30]. The material parameters of the plate and the epoxy film, including density, Young's modulus, Poisson's ratio, and TOE constants listed in Table 1, are defined as the input variables of VUMAT. To model the disbond defect, a seam with different lengths (10 mm, 20 mm, and 40 mm) between the epoxy film and the upper aluminum plate is modeled after a propagation distance of 110 mm from the left end.

A uniform displacement of ten-cycle Hanning windowed sinusoid tone burst with different central frequencies (*i.e.* from 0.10 MHz to 0.45 MHz) is applied on the left end of the plate to excite the probing waves taking the modality of Mode 2, as shown in Figure 4. To warrant the accuracy of the simulation result, a fine mesh with the element length of 0.1 mm (CPE4R) is assigned to the entire model, with a local finer mesh of 0.033 mm (CPE4R) along the thickness direction in epoxy layer. In addition, the infinite element (CINPE4) is assigned to the right-end "wave absorption" region. The out-of-plane displacement is extracted at sampling points and the Short Time Fourier Transform (STFT) is adopted here, which is implemented using a signal processing tool Matlab(R2019b)/stft. To retain sufficient details of both time and frequency information of the signal, a temporal window equivalent of three incident wave periods is selected to intercept acquired signal for FFT. To suppress the signal spectral leakage, each intercepted signal is modulated by the Hanning window. From the obtained spectrogram, one can extract the amplitude of both fundamental and second harmonic UGWs A_1 and A_2. For a further result comparison between simulation and experiment, the respective units of displacement (meter) and voltage (volt) are different. As only the varying trend of the absolute magnitude can be compared, the unit is marked "arbitrary unit" throughout the

investigation.

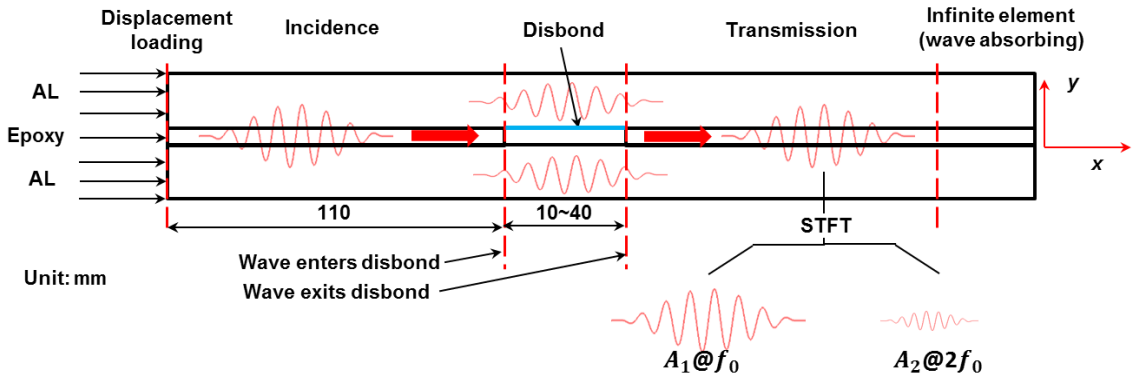

Figure 4 FEM model setup and signal extraction.

3.2. Results and Discussion

3.2.1. Nonlinear Features of UGWs in Intact Multi-layer Waveguide

The simulations for the intact multi-layer bonded waveguide are performed first, with central frequencies of excitation increasing from 0.10 MHz to 0.45 MHz. Figure 5(a) displays the ascertained amplitude of SOHW A_2 (via STFT) when the fundamental frequency $0.10\ \text{MHz} < f_0 < 0.45\ \text{MHz}$ and the propagation distance $1\ \text{cm} < d < 35\ \text{cm}$ in the intact bonded waveguide. As a comparison, the SOHW of Mode S_0 propagating in an Al plate (thickness 1 mm) with identical incident frequencies and propagation distances is investigated as well, as shown in Figure 5(b). From Figure 5, the propagation features of SOHW are extracted and concluded as Table 2.

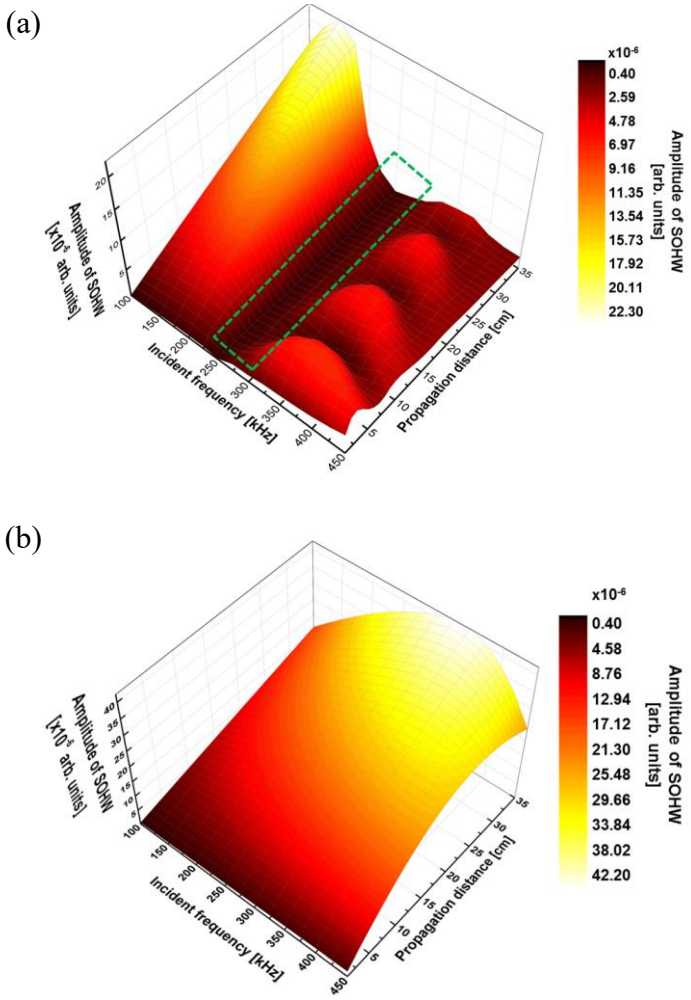

Figure 5 Simulated out-of-plane displacement amplitude of SHOW (obtained via STFT) along propagation direction when the fundamental frequency $\mathbf{0.10\ MHz < f_0 < 0.45\ MHz}$: (a) in bonded Al-epoxy-Al (1 mm – 0.2 mm – 1 mm) waveguide and (b) in single layer Al (1 mm) waveguide.

Table 2 Feature of SOHW in Al-epoxy-Al and Al plate structures

Part	Frequency range	SOHW along propagation distance	Matching mode pair
Al-epoxy-Al (1 - 0.2 - 1 mm)	$0.10\ \text{MHz} < f_0 < 0.225\ \text{MHz}$	Monotonic accumulation	Mode 2 – Mode 2
	$0.225\ \text{MHz} < f_0 < 0.325\ \text{MHz}$	barely noticed with negligible magnitudes	No matching mode pair
	$0.325\ \text{MHz} < f_0 < 0.45\ \text{MHz}$	bounded and oscillated	Mode 2 – Mode 4
Al (1 mm)	$0.10\ \text{MHz} < f_0 < 0.45\ \text{MHz}$	monotonic accumulation	S_0 - S_0

By calibrating the internal resonance requirements, i.e. (1) phase/group velocity matching and (2) non-zero power fluxing, interpretations of the observed features are given as follows. Considering that the probing UGWs take the modality of Mode 2 in the intact bonded waveguide, only the SOHW taking a symmetric modality (i.e. Modes 2 and 4) that satisfies the non-zero power fluxing can be possibly generated. Recalling the dispersive properties analyzed in Section 2, phase/group velocity quasi-matching is satisfied for Mode 2 – Mode 2 with incident frequency $0.10\ \text{MHz} < f_0 < 0.225\ \text{MHz}$, and Mode 2 – Mode 4 with incident frequency $0.325\ \text{MHz} < f_0 < 0.45\ \text{MHz}$. This leads to the monotonic increasing of SOHW in the incident frequency range $0.10\ \text{MHz} < f_0 < 0.225\ \text{MHz}$ and the oscillated amplitude of SOHW in incident frequency range $0.325\ \text{MHz} < f_0 < 0.45\ \text{MHz}$ in Figure 5(a). On the contrary, the fundamental Mode 2 excited at frequency $0.225\ \text{MHz} < f_0 < 0.325\ \text{MHz}$ is unable to find its matching SOHW, and therefore no accumulative SOHW is generated owning to the mode-mismatching, this leading to a minimal amplitude of SOHW with the incident frequency $0.225\ \text{MHz} < f_0 < 0.325\ \text{MHz}$, as highlighted by the rectangle in Figure 5(a). The linear increasing trend of SOHW in the single Al plate is attributable to the matching mode pair S_0- S_0, as proved in several literature [30, 31].

3.2.2. Nonlinear Features of UGWs in Multi-layer Disbonded Waveguide

The incident frequencies are also swept from 0.10 MHz to 0.45 MHz for analyses of nonlinear features of UGWs in multi-layer waveguide with disband defect. Figure 6(a) and (b) exhibit the amplitude of SOHW obtained from the waveguide bearing a disbond of 20 mm length and 40 mm length, respectively. Compared with the results shown in Figure 5(a), the disbond-induced intensification is clearly observed, and for all the excited frequencies, the case with a longer disbond (40 mm) displays a greater intensification of

SOHW in transmitted UGWs than that with a shorter disbond (20 mm). Interpretation of this increase is given in the following. In the disbonded region, the probing UGW of Mode 2 in the intact bonded waveguide is converted to Mode S_0 and Mode 2 propagating in the upper part Al (R_1) and lower part epoxy-Al (R_2) waveguide, respectively. This mode conversion is easily understood considering the similarity of displacement mode shape at an exemplary frequency $f_0 = 0.3$ MHz, as displayed in Figure 7, and a detailed investigation of mode conversion is performed in Ref. [11]. Both converted fundamental UGWs satisfy the internal resonance requirements in the incident frequency range 0.10 MHz $< f_0 <$ 0.45 MHz, and therefore lead to the generation of accumulative SOHW, as evidenced in Figure 5(b). Upon transmitting from the disbonded region to the bonded waveguide, these accumulated SOHW (Mode S_0 and Mode 2 at $2f_0$ in the regions R_1 and R_2, respectively) are converted to SOHW at $2f_0$ in the bonded waveguide. As a result, this leads to the increase in the measured amplitude of SOHW in probing waves.

(a)

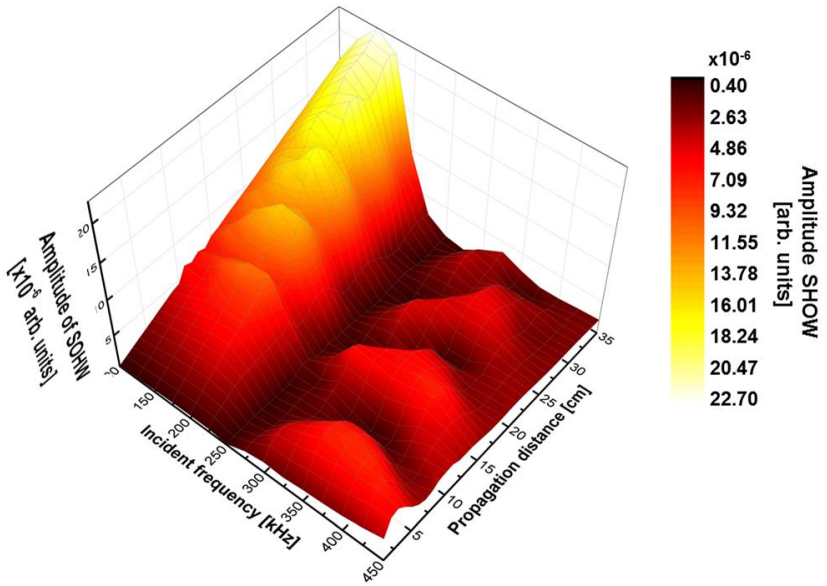

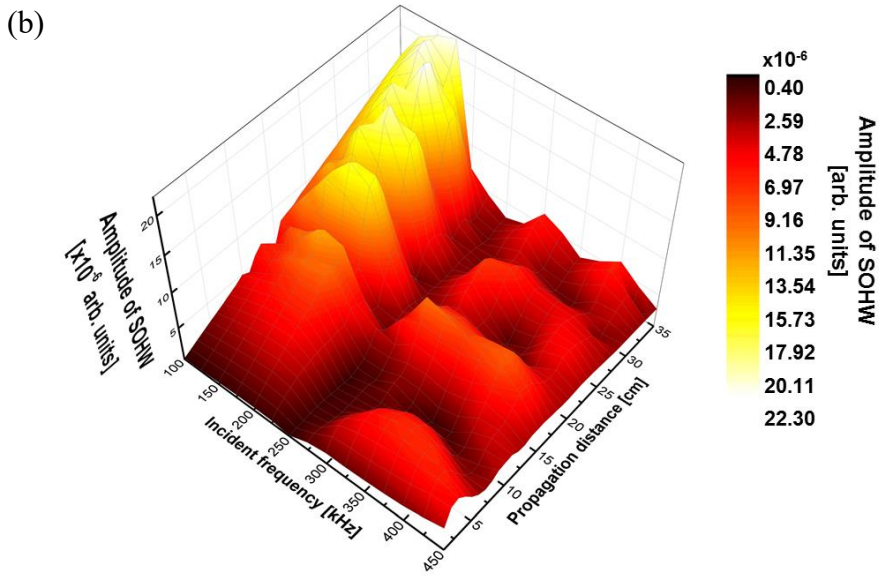

Figure 6 Simulated out-of-plane displacement amplitude of SOHW (obtained via STFT) along propagation direction when the fundamental frequency $\mathbf{0.1\ MHz < f_0 < 0.45\ MHz}$: in the Al-epoxy-Al waveguide with disbond of (a) 20 mm and (b) 40 mm.

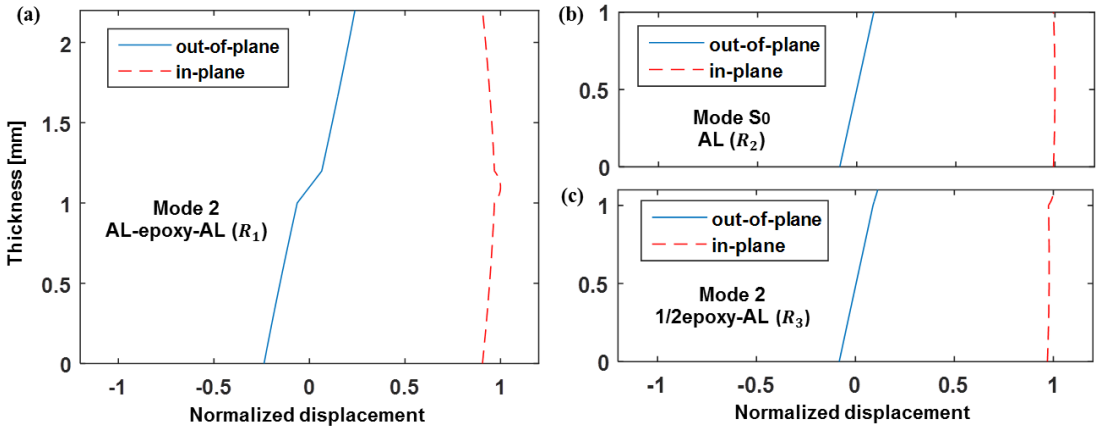

Figure 7 Wave displacement mode shape along the thickness direction at 0.3 MHz (a) mode 2 at bonded waveguide $\boldsymbol{R_1}$, (b) mode $\boldsymbol{S_0}$ at disbonded waveguide $\boldsymbol{R_2}$, and (c) mode 2 at disbonded waveguide $\boldsymbol{R_3}$.

Considering that the amplitude of SOHW in the intact waveguide varies dramatically against the incident frequency (see Figure 5(a)), the extent of the disbond-induced change in the SOHW manifest phenomenal discrepancies in accordance with the incident frequency. Figure 8(a) and (b) exhibits the ratio of the disbond-induced increase in the

amplitude of SOHW to the counterpart obtained in an intact bonded waveguide. It is clearly observed that only when the probing wave of Mode 2 is excited at $0.225\ \text{MHz} < f_0 < 0.325\ \text{MHz}$, the disbond-induced SOHW overwhelms the counterpart induced by the intrinsic material nonlinearity in the intact region, as highlighted by the rectangle in Figure 8. This is because in this incident frequency range, the generation of SOHW in intact region is remarkably suppressed owning to the mode-mismatching as analyzed above, and therefore the SOHW generated in the disbond region is predominant. This phenomenon provides the basis for the selection of probing wave mode with the potential of outstanding the disbond-induced SOHW.

(a)

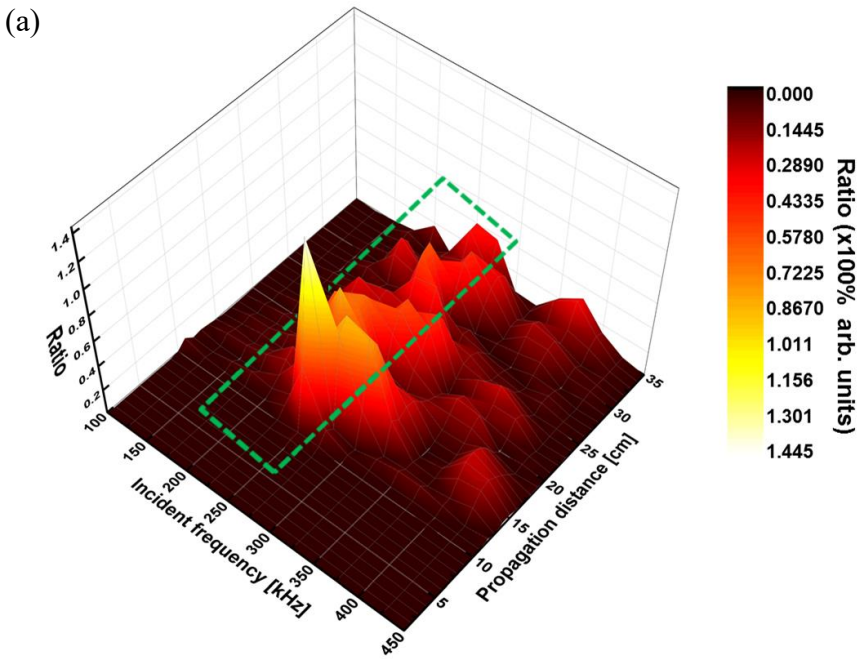

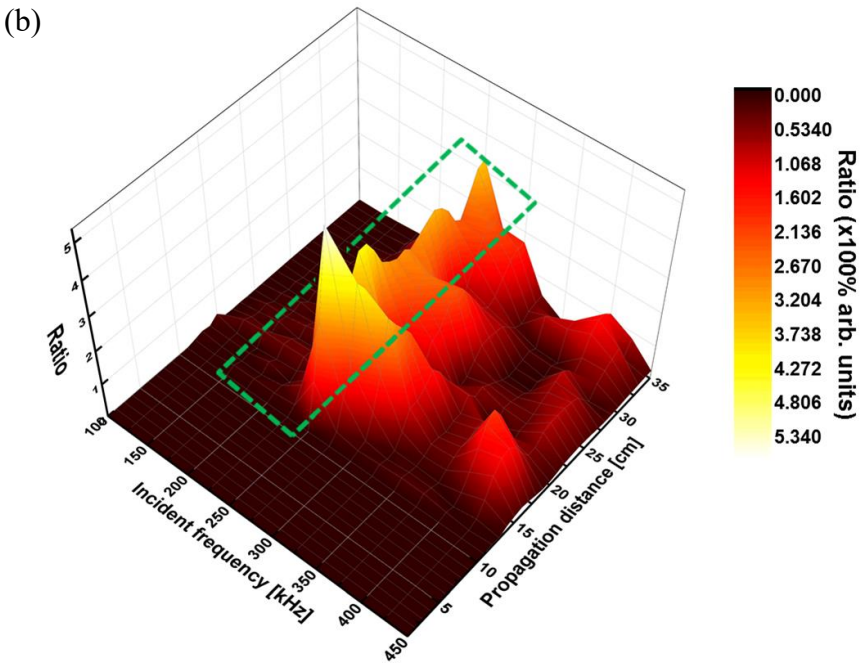

Figure 8. Ratio of disbond-induced increase in amplitude of SOHW to the counterparts in the intact bonded waveguide: in the Al-epoxy-Al waveguide with disbond of (a) 20 mm and (b) 40 mm.

As a representation, the incident UGW at $f_0 = 0.3$ MHz featuring mode-mismatching is selected to probe the bonded waveguide, because at this mode-frequency combination, the SOHW in the intact waveguide is of low magnitude (see Figure 5(a)). By contrast, if a disbond is produced, the UGWs propagating in the disbonded region are converted to Mode S_0 in R_1 and Mode 2 in R_2 (see Figure 9(a)), and these modes result in the generation of accumulative SOHW (see Figure 9(b)) from Interface I to Interface II. This SOHW induced by the disbond overwhelms the counterpart from intact waveguide which is suppressed at the selected f_0. In addition, the increase of disbond length leads to the augmentation of disbond-related SOHW, which enables the potential of quantitative characterization of disbond.

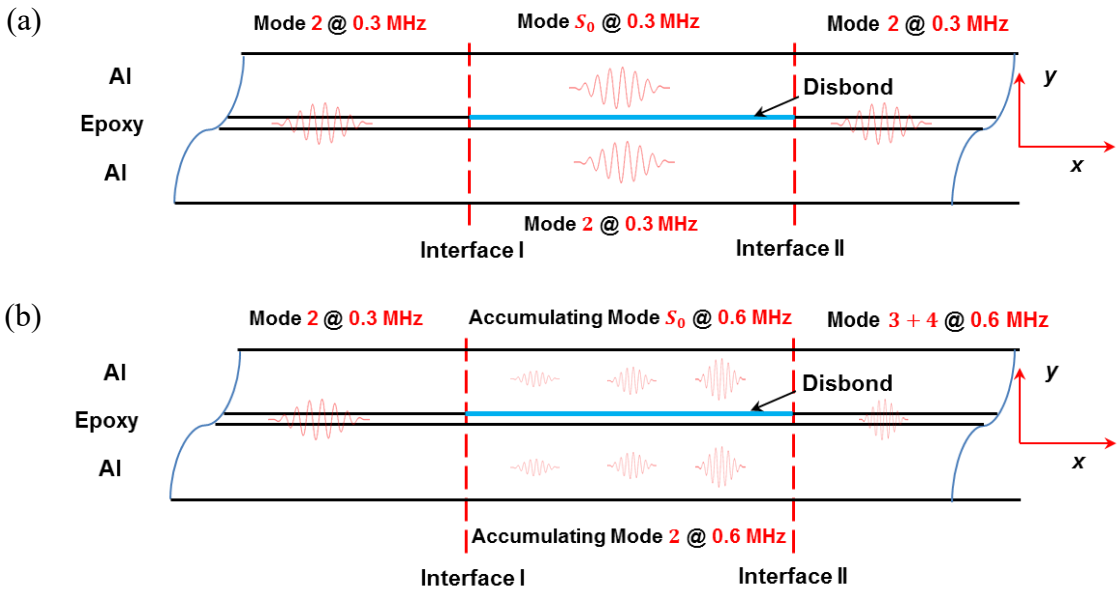

Figure 9 When Mode 2 at 0.3 MHz is excited, (a) schematic illustration of disbond-induced mode conversion; (b) disbond-induced SOHW in UGW.

It is worth noting that at this representative excitation frequency (i.e. $f_0 = 0.3$ MHz) after transmitting through the disbonded region, the disbond-induced SOHW manifests an oscillating trend along wave propagation (Figure 10). This is because in the disbonded region, the accumulated SOHW of Mode S_0 and Mode 2 at the respective Al layer and epoxy-Al layer have slightly different phase velocity, as shown in Figure 3(a), and this leads to the relative phase asynchronization of both stress and displacement distribution at the interface II compared with that at interface I. Attributed to the asynchronization, the accumulative SOHW propagating through the disbond at interface II are converted to Mode 3 and Mode 4 at the intact region. These two modes, with slightly different phase velocities, add constructively and destructively along the propagation distance from Interface II to form the beat effect [32], leading to the oscillating trend of the disbond-induced SOHW in Figure 10.

In practical application, since the transducer that is used to capture the probing waves is

of a finite width, the wave signals recorded are, in essence, the superposition of wave signals from all sensing points in the region covered by the transducer. This alludes to the fact that the minimum amplitude of disbond-induced SOHW captured by the transducer is remarkably greater than the counterpart from the intact waveguide, and this guarantees the applicability of the disbond-induced SOHW to disbond characterization.

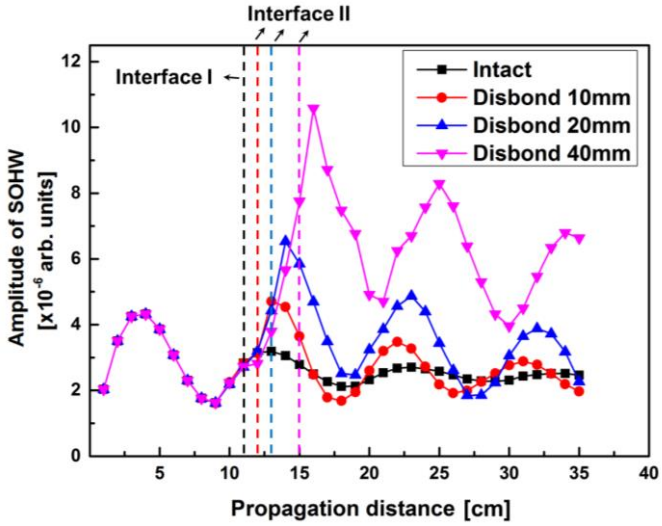

Figure 10 Simulated out-of-plane displacement amplitude of SOHW (obtained via STFT) along propagation direction in intact waveguide and waveguide bearing disbond of 10 mm, 20 mm and 40 mm length.

From all the above simulation results, it is clearly observed that the disbond causes a conspicuous increase in the SOHW, demonstrating good coincidence with the theoretical analysis. Hence, provided that the UGW Mode 2 at the optimal frequency (*i.e.* $f_0 = 0.3$ MHz in this study) featuring mode-mismatching is used to probe a multi-layer bonded waveguide, the nonlinearity in UGWs can be used as an indicator for the disbond defect evaluation.

4. Experimental Sizing of Disbond Defect

4.1. Test Setup

For proof of concept of the proposed method, a multi-layer bonded waveguide is prepared in which two 300 mm × 300 mm aluminum plates measuring 1 mm in thickness are bonded using an epoxy film (Hysol® PL7000) with a uniform thickness of 0.2 mm. In this structure, artificial disbond defects are introduced by placing Teflon inserts between one Al plate and the epoxy sheet adhesive, forming unbonded surfaces. A photograph of the specimen is shown in Figure 11(a). The size of the defect is 10 mm × 10 mm, 20 mm × 20 mm and 40 mm × 40 mm for the disbond denoted by D1, D2, and D3, respectively.

To investigate the generation of nonlinearity of UGWs, a ten-cycle Hanning-window modulated sinusoidal tone burst at a central frequency of 0.3 MHz is generated using a computer controlled system (Ritec® 5000 SNAP) to excite the probing waves. Two piston piezoelectric transducers (ø25.4 mm) with respective central frequencies of 0.3 MHz and 0.6 MHz (as actuator and receiver, respectively) are coupled with the specimen, as shown in Figure 11(a). A couplant (Olympus® Glycerin) is applied to ensure a consistent coupling when the transducers are scanning the waveguide. The skew angles for the actuator and receiver are set to be 30 degree, which is obtained using the Snell's law [33], to preferably generate Mode 2 at 0.3 MHz.

The nonlinear feature of UGWs generated in a single layer aluminum plate is first examined. The distance between the actuator and the receiver is increased from 10 mm to 120 mm with an increment of 10 mm. Similar tests are performed on the multi-layer bonded structures with and without disbond defects.

To calibrate the nonlinearity in the waveguide, a relative acoustic nonlinearity parameter (RANP) β is defined as

$$\beta = \frac{A_2}{A_1^2}, \tag{1}$$

where A_2 and A_1 denote the amplitude of the SOHW and fundamental mode, respectively [34].

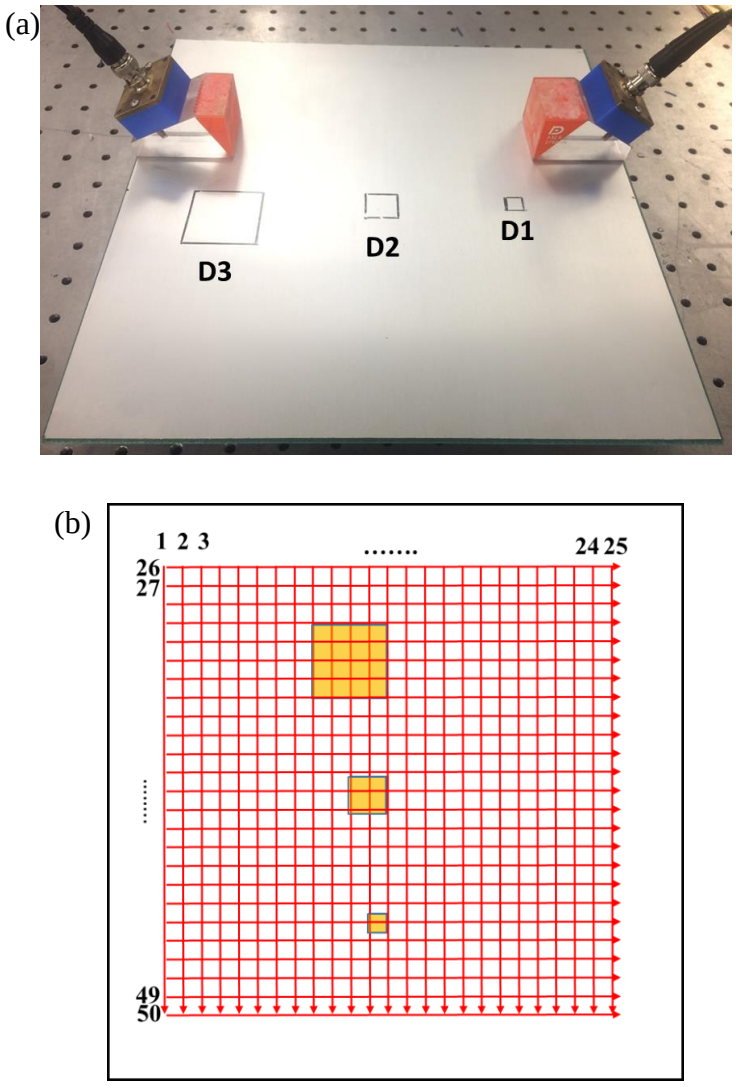

Figure 11 (a) Photograph of the specimen and the angle beam transducers; and (b) schematic of disbond defect evaluation through 50 scanning paths.

4.2. Nonlinear Feature of UGWs in Aluminum Plate and Intact Bonded Waveguide

In the single layer Al plate, the Mode S_0 is observed to dominate the wave energy. From the acquired wave signals, the amplitudes of fundamental and second harmonic modes can be extracted using the STFT, with which the nonlinearity index β is obtained, as displayed in Figure 12. The average value and error bar which represents the standard deviation are calculated according to four repeated experiments. The ascertained β shows an approximately linear increase with the propagation distance, and this corroborates the numerical result in Section 3.2.1.

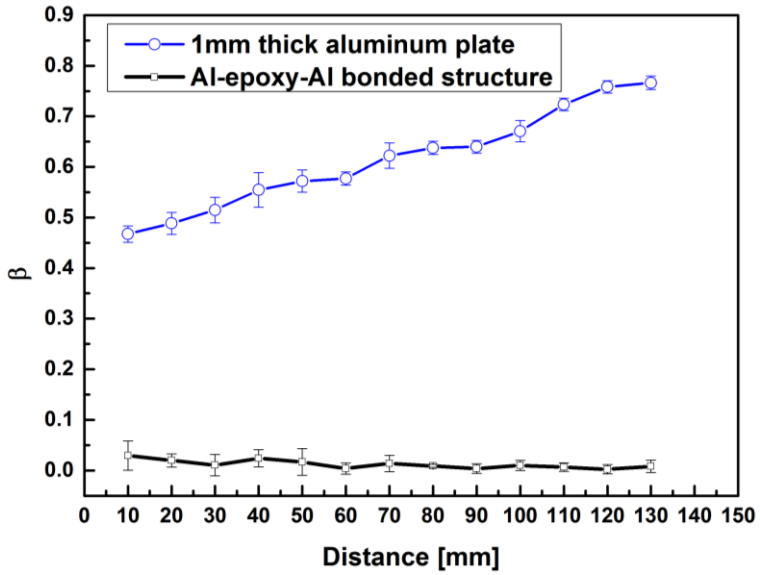

Figure 12 Value of RANP extracted in four repeated experiments.

Likewise, in the intact bonded region, the probing waves of Mode 2 is observed to occupy the dominant energy, and the extracted SOHW through STFT (Figure 12) manifests a fairly low amplitude. Showing good agreement with the results from numerical method, this validates the suppression of SOHW accumulation in the intact bonded waveguide when Mode 2 at the selected frequency (i.e. 0.3 MHz) is excited, owing to the mode-

mismatching (i.e. phase/group velocity mismatching) between SOHW and the fundamental Mode 2, as analyzed in Section 3.2.1.

4.3. Disbond Evaluation using Nonlinear Features

With the experimentally validated nonlinear features of UGWs in the intact bonded waveguide, the nonlinear features of UGWs in the waveguide with three pre-embedded disbonds are interrogated, as shown in Figure 11(a), to examine the disbond-induced SOHW. A ten-cycle Hanning-window modulated sinusoidal tone burst at a central frequency of 0.3 MHz is applied to generate Mode 2 as the fundamental wave. To probe the specimen, 50 scanning paths are defined (see Figure 11(b)), where the actuator and receiver move in parallel 10 mm each time, to enclose a monitoring area of 250 mm × 250 mm.

Both the fundamental and second harmonic modes are extracted from the acquired UGWs using the STFT. Figure 13 representatively shows the spectra of wave signals captured from paths which traverse the intact region and disbonded region with disbond length of 10 mm, 20 mm and 40 mm, respectively. It is clearly observed that, with the mode-matching in the disbond region, increase of SOHW in the probing UGWs is induced, as highlighted by the rectangles in Figure 13. Exemplarily, a respective increase of 378% for sensing path traversing a 40 mm disbond and 188% for sensing path traversing a 20 mm disbond is observed in comparison with that from the sensing path 42 which traverses the intact region.

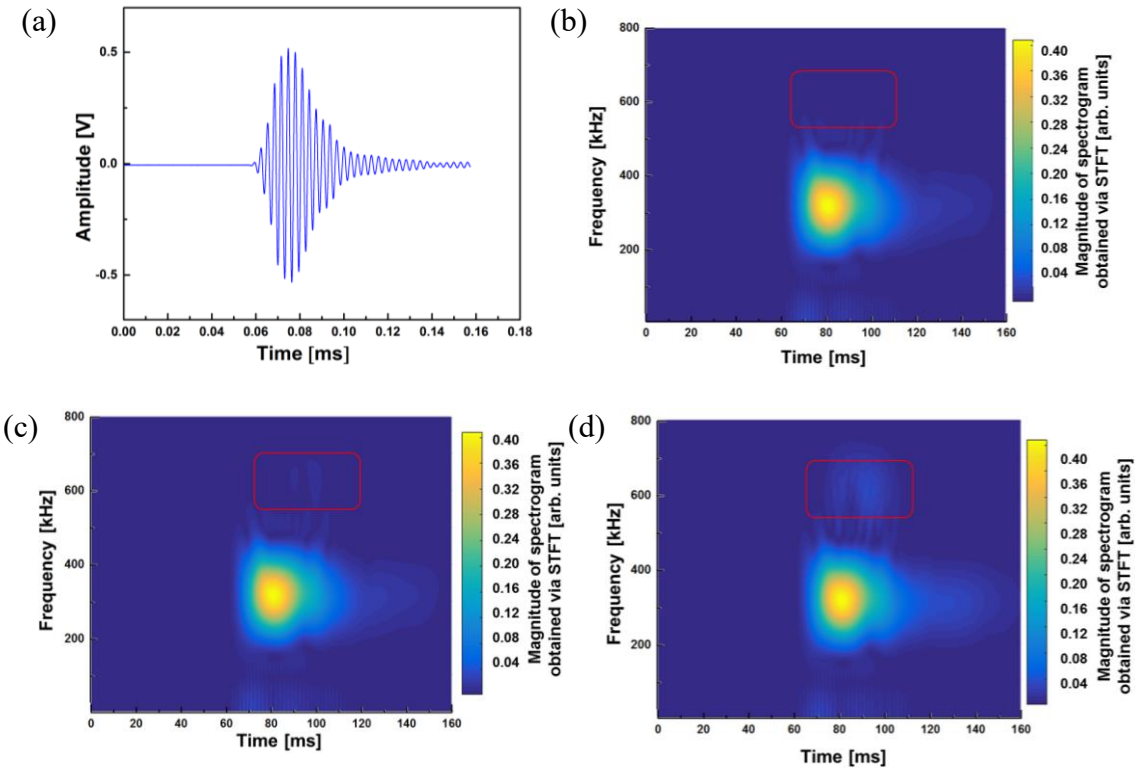

Figure 13 (a) Representative signal acquired via the transducer; spectra of signals obtained using STFT via (b) path 42 (intact); (c) path 37 (disbond 20 mm); and (d) path 30 (disbond 40 mm).

The calculated parameter β can be used as damage indices (DIs) to highlight the path with disbond defect (see Figure 14(a)), indicating the existence of disbond defect. In addition, just as analyzed theoretically and numerically, the experimentally obtained value of β increases with the enlargement of disbond defect length. Particularly, due to the accumulative contribution to the SOHW from all the three disbond defects, the corresponding path 12 shows a largest value of β. With the ascertained β from the 50 scanning paths, a typical imaging method, the reconstruction algorithm for probabilistic inspection of damage (RAPID)[35], can be readily exploited to intuitively show both the location of the disbonds and their severity (see Figure 14(b)). The imaging result shows good coincidence with the reality, validating the effectiveness of the nonlinear features in the UGWs of prudentially selected mode.

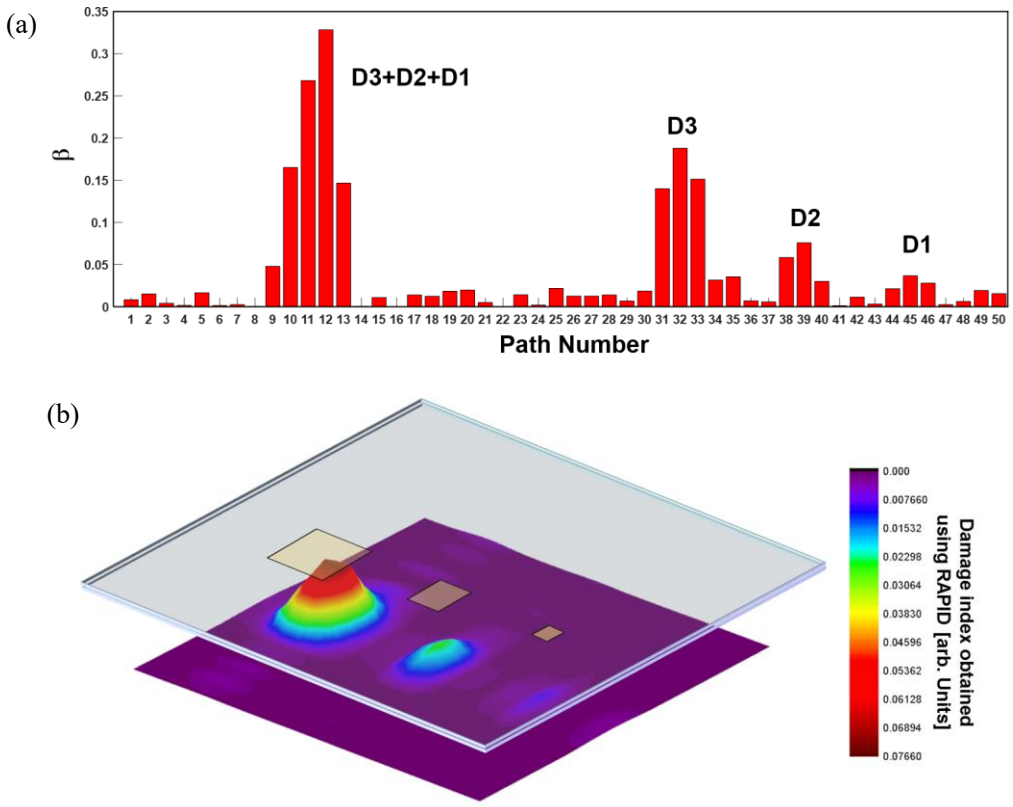

Figure 14 (a) Value of RANP on the 50 paths in experiment; (b) imaging result of disbond in a multi-layer bonded structure using the RAPID algorithm.

5. Conclusions

An investigation on nonlinear features of UGWs in a metallic bonded waveguide is performed in this study, and the effect of disbond on nonlinear features of UGWs is scrutinized, on which basis the disbond evaluation can be fulfilled by making use of an optimal UGW mode featuring mode-mismatching. In this investigation, the dispersion curves of the bonded structure are obtained with a global matrix method, and the nonlinear features of UGWs in the bonded structure and the disbonded region is analyzed from a numerical perspective. It is demonstrated that the structural traits at the disbonded region can lead to the intensification of nonlinear features in probing UGWs. Provided UGWs of a prudently selected mode-frequency combination (*i.e.*, Mode 2 - 0.3 MHz in the case

studied) are excited, the disbond-induced SOHW overwhelms the counterpart generated in the intact waveguide. Based on this characteristic, a method using the SOHW is proposed, which is capable of outstanding and evaluating the disbond defect. Experimental results demonstrate the effectiveness of the proposed disbond evaluation method.

It is noteworthy that the effectiveness of the proposed method lies in the fact that, at the disbond defect, the unbonded surfaces between the adhesive and the adherend transmit no shear stress, so that the UGWs in each separated layer can propagate independently. This alludes to the fact that the proposed method can be potentially applied to the evaluation of the kissing bond, which is of critical science and practical importance. This is because the kissing bond features the tiny and ignorable shear stiffness at the defect as well, and therefore, it will induce the intensification of nonlinear features in UGWs in a similar manner to that in the scenario of disbond defect. The application of the proposed method to the evaluation of the kissing bond will be explored in the future work.

Acknowledgement

Zhongqing Su would like to acknowledge the support from the Hong Kong Research Grants Council via a General Research Fund (Nos.:15201416 and 15212417) and from the National Natural Science Foundation of China (No. 51635008). Fangsen Cui wants to thank the Institute of High Performance Computing for the use of computational resources to carry out this research.

References

[1] Higgins A. Adhesive bonding of aircraft structures. *Int J Adhes Adhes* 2000; 20: 367–376.

[2] Chester RJ, Walker KF, Chalkley PD. Adhesively bonded repairs to primary aircraft structure. *Int J Adhes Adhes* 1999; 19: 1–8.
[3] Adams RD. *Adhesive bonding: science, technology and applications*. Elsevier, 2005.
[4] Wikipedia. Aloha Airlines Flight 243, https://en.wikipedia.org/wiki/Aloha_Airlines_Flight_243 (2018, accessed 4 August 2018).
[5] Drinkwater B, Cawley P. Measurement of the frequency dependence of the ultrasonic reflection coefficient from thin interface layers and partially contacting interfaces. *Ultrasonics* 1997; 35: 479–488.
[6] Brotherhood CJ, Drinkwater BW, Dixon S. The detectability of kissing bonds in adhesive joints using ultrasonic techniques. *Ultrasonics* 2003; 41: 521–529.
[7] Garnier C, Pastor M-L, Eyma F, et al. The detection of aeronautical defects in situ on composite structures using Non Destructive Testing. *Compos Struct* 2011; 93: 1328–1336.
[8] Su Z, Ye L, Lu Y. Guided Lamb waves for identification of damage in composite structures: A review. *J Sound Vib* 2006; 295: 753–780.
[9] Ren B, Lissenden CJ. Modal content-based damage indicators for disbonds in adhesively bonded composite structures. *Struct Heal Monit* 2016; 15: 491–504.
[10] Matt H, Bartoli I, Lanza di Scalea F. Ultrasonic guided wave monitoring of composite wing skin-to-spar bonded joints in aerospace structures. *J Acoust Soc Am* 2005; 118: 2240–2252.
[11] Puthillath P, Galan JM, Ren B, et al. Ultrasonic guided wave propagation across waveguide transitions: Energy transfer and mode conversion. *J Acoust Soc Am* 2013; 133: 2624–2633.
[12] Ong WH, Rajic N, Chiu WK, et al. Lamb wave--based detection of a controlled disbond in a lap joint. *Struct Heal Monit* 2018; 17: 668–683.
[13] Zhuang Y, Kopsaftopoulos F, Dugnani R, et al. Integrity monitoring of adhesively bonded joints via an electromechanical impedance-based approach. *Struct Heal Monit* 2018; 17: 1031–1045.
[14] Malinowski P, Ostachowicz WM, Brune K, et al. Study of electromechanical impedance changes caused by modifications of CFRP adhesive bonds. *Fatigue Fract Eng Mater Struct* 2017; 40: 1592–1600.
[15] Quaegebeur N, Micheau P, Masson P, et al. Methodology for optimal configuration in structural health monitoring of composite bonded joints. *Smart Mater Struct* 2012; 21: 105001.
[16] Puthillath P, Rose JL. Ultrasonic guided wave inspection of a titanium repair patch bonded to an aluminum aircraft skin. *Int J Adhes Adhes* 2010; 30: 566–573.
[17] Wang K, Liu M, Cao W, et al. Detection and sizing of disbond in multilayer bonded structure using modally selective guided wave. *Struct Heal Monit*.
[18] Chillara VK, Lissenden CJ. Review of nonlinear ultrasonic guided wave nondestructive evaluation: theory, numerics, and experiments. *Opt Eng* 2015; 55: 011002.

[19] Mandal DD, Banerjee S. Identification of breathing type disbonds in stiffened panels using non-linear Lamb waves and built-in circular PWT array. *Mech Syst Signal Process* 2018; (under rev: 33–51.
[20] Yan D, Neild SA, Drinkwater BW. Modelling and measurement of the nonlinear behaviour of kissing bonds in adhesive joints. *NDT E Int* 2012; 47: 18–25.
[21] Chen BY, Soh SK, Lee HP, et al. A vibro-acoustic modulation method for the detection of delamination and kissing bond in composites. *J Compos Mater* 2016; 50: 3089–3104.
[22] Carrino S, Nicassio F, Scarselli G. Subharmonics and beating: A new approach to Local Defect Resonance for bonded single lap joints. *J Sound Vib* 2019; 456: 289–305.
[23] He S, Ng CT. Modelling and analysis of nonlinear guided waves interaction at a breathing crack using time-domain spectral finite element method. *Smart Mater Struct* 2017; 26: 85002.
[24] Shen Y, Wang J, Xu W. Nonlinear features of guided wave scattering from rivet hole nucleated fatigue cracks considering the rough contact surface condition. *Smart Mater Struct* 2018; 27: 105044.
[25] Shen Y, Cesnik CES. Modeling of nonlinear interactions between guided waves and fatigue cracks using local interaction simulation approach. *Ultrasonics* 2017; 74: 106–123.
[26] De Lima WJNN, Hamilton MF. Finite-amplitude waves in isotropic elastic plates. *J Sound Vib* 2003; 265: 819–839.
[27] Leckey C, Hinders M. 3D modeling of ultrasonic wave interaction with disbonds and weak bonds. *AIP Conf Proc* 2012; 1430: 111–117.
[28] Ludwig R, Sullivan JM, Dai D. Ultrasonic NDE of Adhesive Metal to Metal Bond Integrity Based on a Combined Numerical and Expert System Approach. *Rev Prog Quant Nondestruct Eval* 1993; 12: 1555–1562.
[29] Lowe MJS. Matrix Techniques for Modeling Ultrasonic-Waves in Multilayered Media. *Ieee Trans Ultrason Ferroelectr Freq Control* 1995; 42: 525–542.
[30] Liu M, Wang K, Lissenden CJ, et al. Characterizing hypervelocity impact (HVI)-induced pitting damage using active guided ultrasonic waves: From linear to nonlinear. *Materials (Basel)*; 10. Epub ahead of print 2017. DOI: 10.3390/ma10050547.
[31] Zuo P, Zhou Y, Fan Z. Numerical and experimental investigation of nonlinear ultrasonic Lamb waves at low frequency. *Appl Phys Lett*; 109. Epub ahead of print 2016. DOI: 10.1063/1.4958705.
[32] Ti BW, O'Brien Jr WD, Harris JG. Measurements of coupled Rayleigh wave propagation in an elastic plate. *J Acoust Soc Am* 1997; 102: 1528–1531.
[33] Rose JL. *Ultrasonic guided waves in solid media*. Cambridge university press. Epub ahead of print 2014. DOI: 10.1017/CBO9781107273610.
[34] Müller MF, Kim J-Y, Qu J, et al. Characteristics of second harmonic generation of Lamb waves in nonlinear elastic plates. *J Acoust Soc Am* 2010; 127: 2141–2152.
[35] Zhao X, Qian T, Mei G, et al. Active health monitoring of an aircraft wing with an

embedded piezoelectric sensor/actuator network: II. Wireless approaches. *Smart Mater Struct* 2007; 16: 1218–1225.